Diamond-Type Lipid Cubic Phase with Large Water Channels

ARTICLE *in* JOURNAL OF THE AMERICAN CHEMICAL SOCIETY · JULY 2003

Impact Factor: 12.11 · DOI: 10.1021/ja034578v · Source: PubMed

J|A|C|S
COMMUNICATIONS

Published on Web 05/20/2003

Diamond-Type Lipid Cubic Phase with Large Water Channels

Borislav Angelov,† Angelina Angelova,‡ Michel Ollivon,*,§ Claudie Bourgaux,⊥ and Andrew Campitelli‡

Institute of Biophysics, Bulgarian Academy of Sciences, Acad. G.Bonchev Str. Bl.21, BG-1113 Sofia, Bulgaria, Biosensors group, IMEC, Kapeldreef 75, B-3001 Leuven, Belgium, CNRS UMR 8612, 92296 Châtenay, France, and LURE, Université Paris-Sud, F-91898 Orsay, France

Received February 9, 2003; E-mail: michel.ollivon@cep.u-psud.fr

This paper describes a diamond cubic phase with large water channels and determines the temperature dependence of the bilayer thickness in the cubic monoolein/octylglucoside/water system based on time-resolved synchrotron X-ray diffraction data. The X-ray diffraction study evidences a diamond-type lipid cubic phase, D_{large}, with large water channels (6.98 nm water core diameter at 20 °C), which has not been previously reported. It is a distinct phase, different from the diamond cubic phase D_{normal} with normal water channels (2.96 nm water core at 70 °C). The larger channels might allow an enhanced entrapment efficiency of biomolecules in lipid cubic phases. The X-ray diffraction patterns recorded during a thermal scan showed a cubic−cubic structural transition from D_{large} to D_{normal}. The obtained cubic phases displayed much larger lattice spacings (a = 15.3 nm at 20 °C) as compared to those of pure monoolein at full hydration (a = 10.7 nm at 20 °C).

Following the pioneering works on crystallography,[1] mathematical description,[2] and a physical model[3] of lipid cubic phases, it has been found that membrane proteins can be effectively crystallized in such nonlamellar media.[4] Bicontinuous cubic phases have significant features favoring their growing use in biophysical and biomedical fields, and in food and cosmetics industries. Structural and chemical advantages of the lipid cubic phases include highly ordered periodic structures, a large surface area of the lipid/water interface (on the order of 400 m^2/g),[5a] bicontinuous or cubosome textures, and biocompatible media for entrapment of proteins, peptides, and other biomolecules. To utilize these properties, various applications are being developed such as controlled drug delivery systems, biosensors,[5b] and nanostructured composite biomaterials.

Monoolein (MO)/detergent systems may form stable cubic phases for membrane protein crystallization.[4] To understand the structural stability of nonlamellar amphiphilic systems[6,7] as influenced by detergents,[8,9] the lipid bilayer thickness in the cubic phase[10] should be determined. The latter would allow one to estimate the sizes of the water compartments accommodated inside the cubic unit cell. The bilayer and the water channel thicknesses are structural parameters of great practical importance for protein entrapment and membrane protein reconstitution in lipid cubic phases.

Previously reported X-ray diffractograms of cubic lipid/water systems have been mostly explored for symmetry characterization. The structural complexity of the underlying minimal surface and the large number of molecules per unit cell (about 500 molecules for the case of MO)[11] have hampered the in-depth study of the X-ray data. A simplified model for analysis of scattering patterns of self-assembled cubic phases has been recently proposed by Garstecki and Holyst[10] (GH model). It is an insightful continuation of the works of Clerc and Dubois-Violette[12] and Harper and Gruner[13] and requires fitting of model intensity curves to experimental ones.

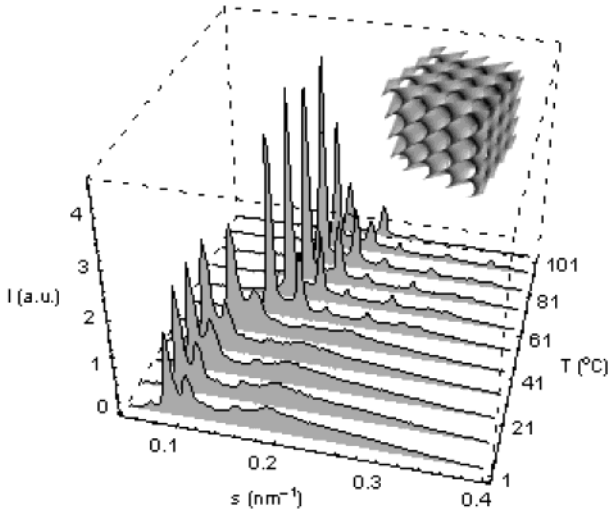

Figure 1. Time-resolved X-ray diffraction patterns of hydrated MO/OG mixture (90/10, mol/mol) showing a transition between diamond cubic phases ($D_{large} \rightarrow D_{normal}$) upon heating. Inset: *Pn*3*m* lattice.

Here we investigate the temperature dependence of the lipid bilayer thickness in a MO cubic phase incorporating a small amount of octylglucoside (OG). A powder of 1-monooleoyl-*rac*-glycerol (purity >99.5%) was hydrated and dispersed in excess aqueous phase containing 0.095 M *n*-octyl β-D-glucopyranoside (purity >99.5%) in 0.1 M NaCl (phosphate buffer pH 7.0), yielding a lipid-to-detergent molar ratio of 90/10. This molar ratio between MO and OG was chosen to be close to the critical value for the induction of a nonlamellar-to-lamellar phase transition in MO, which was estimated in our previous work.[8] The structure of the lipid/detergent/water mixture was studied by means of synchrotron X-ray diffraction. Figure 1 shows time-resolved X-ray diffraction patterns recorded in the SAXS region in the interval from 1 to 100 °C. The sample was scanned at a rate 2 °C/min at beamline D24 of LURE (Orsay, France). The principle of the experimental setup is analogous to that described in refs 8 and 14. We present one-dimensional X-ray diffractograms as intensities vs reciprocal spacings (s) for selected temperatures. The patterns define periodic 3D structures with diamond *Pn*3*m* cubic lattices (Figure 1). The characteristic X-ray diffraction peaks with reciprocal spacings spaced in the ratio $\sqrt{2}:\sqrt{3}:\sqrt{4}:\sqrt{6}:\sqrt{8}:\sqrt{9}:\sqrt{10}:\sqrt{12}:\sqrt{14}$ ... were used for the determination of the *Pn*3*m* cubic lattice parameter a.

A detailed analysis of the time-resolved X-ray diffraction patterns was performed at every 2° of the scan from 1 to 100 °C. The lipid bilayer thickness, L, and the dimensionless bilayer thickness ratio, L/a, were determined explicitly from the experimental X-ray data

† Bulgarian Academy of Sciences.
‡ IMEC.
§ CNRS UMR 8612.
⊥ LURE.

10.1021/ja034578v CCC: $25.00

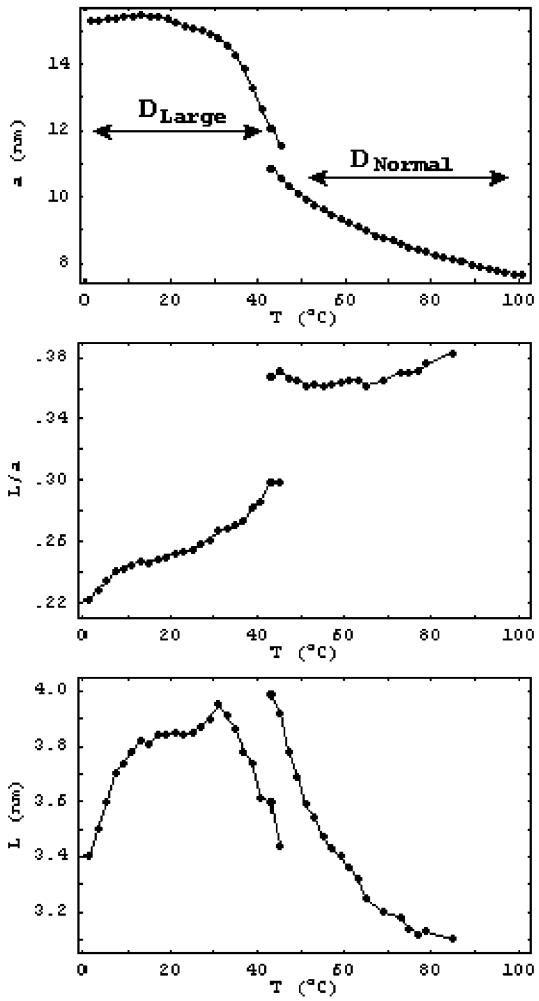

Figure 2. Temperature dependences of the unit cell constant *a*, the dimensionless bilayer thickness *L*/*a*, and the bilayer thickness *L* in MO/OG (90/10, mol/mol) cubic phase. The *Pn*3*m* spacegroup keeps throughout. The transition $D_{large} \rightarrow D_{normal}$ occurs at 44 °C.

using the GH model[10] and our procedure for intensity curve fitting (see the Supporting Information). The intensities of the diffraction patterns were calculated by formula (7) from ref 10b. The simultaneously fitted parameters were the following: (1) the dimensionless bilayers thickness *L*/*a*; (2) the *s* value of the first peak that best optimizes the *s* values of the first six peaks of the *Pn*3*m* structure; (3) the peak width (the *Pn*3*m* peaks were supposed to be Gaussian peaks of equal width); (4) the intensity of the first peak that best optimizes the intensities of the first six *Pn*3*m* peaks; (5) another four parameters were added to model a coexistence of *Im*3*m* and *Pn*3*m* phases or of two *Pn*3*m* phases during the phase transitions; (6) the background was modeled as a Gaussian peak with three parameters. The transition $D_{large} \rightarrow D_{normal}$ was thus modeled by 11 parameters. To better fit the small-intensity peaks from the third to sixth reflection, we worked with logarithmic intensities. The obtained temperature dependencies of the cubic lattice parameter, the dimensionless bilayer thickness, and the thickness of the lipid bilayer are presented in Figure 2.

We verified that the MO/OG/water system displays a *Pn*3*m* cubic symmetry over the entire interval from 1 to 100 °C. Around 44 °C, a cubic−cubic transition from *Pn*3*m* (D_{large}) to *Pn*3*m* (D_{normal}) is established (Figure 2). At temperature below 5 °C, superimposed reflections of *Im*3*m* and *Pn*3*m* cubic phases were resolved, the intensity of the strongest *Im*3*m* peak being nearly 10 times smaller than that of the strongest *Pn*3*m* peak. A third isotropic phase, modeled as a single broad Gaussian peak, was well resolved for every temperature at *s*-maximum in the interval $s \sim 0.20 \div 0.25$ nm^{-1}. Such background scattering was interpreted as a disordered bicontinuous phase.[10b] If some amount of OG separates from MO to form micelles, a typical maximum for OG micelles at $s \sim 0.34$ nm^{-1} would be observed. The micellar maximum could shift to $s \sim 0.27 \div 0.37$ nm^{-1} if mixed lipid/OG micelles[15] were formed. Considering that the isotropic ("disordered") phase in the present system displays a peak maximum at $s < 0.25$ nm^{-1}, we conclude that OG micelles are not formed. Hence, the obtained results suggest that the detergent OG homogeneously mixes with MO at a molar ratio of 90/10. The shape of the X-ray patterns changes notably on heating at around 44 °C during the transition $D_{large} \rightarrow D_{normal}$ (Figure 1). The intensity of the isotropic disordered phase decreased by about 50% for the normal *Pn*3*m* structure (D_{normal}) as compared to that for the cubic phase with large water channels (D_{large}).

The variation of the bilayer thickness and the remarkable features of the $D_{large} \rightarrow D_{normal}$ cubic−cubic structural transition are reported here for the first time (Figure 2). The induction of D_{large} is associated with a disorder in the bicontinuous structure resulting from the dilatation of the water channels caused by OG. The downward jump of the lattice parameter *a* around 44 °C could be due to changes in the OG solubility upon increasing temperature (OG cmc ~ 25 mM at 25 °C). This reduces the hydration of D_{large}, and thus a portion of the phase transforms into an ordered D_{normal} structure. The presented structural information is important for the entrapment of proteins in lipid nanochannel networks as well as for the studies on stability of cubic phases.[6,7] The results suggest that addition of 10 mol % of OG to MO considerably increases the hydration of the lipid cubic phase without causing a phase transformation into a lamellar phase.

Supporting Information Available: Details on X-ray data analysis for experimental results at selected temperatures. This material is available free of charge at http://www.pubs.acs.org.

References

(1) (a) Luzzati, V.; Spegt, P. A. *Nature* **1967**, *215*, 701. (b) Longley, W.; McIntosh, T. J. *Nature* **1983**, *303*, 612.
(2) (a) Scriven, L. E. *Nature* **1976**, *263*, 123. (b) Schnering, H.; Nesper, R. *Z. Phys. B* **1991**, *83*, 407.
(3) (a) Sadoc, J. F.; Charvolin, J. *J. Phys.* **1986**, *47*, 683. (b) Charvolin, J.; Sadoc, J. F. *J. Phys.* **1987**, *48*, 1559. (c) Charvolin, J.; Sadoc, J. F. *J. Phys.* **1988**, *49*, 521.
(4) (a) Landau, E. M.; Rosenbusch, J. P. *Proc. Natl. Acad. Sci. U.S.A.* **1996**, *93*, 14532. (b) Nollert, P.; Navarro, J.; Landau, E. M. *Methods Enzymol.* **2002**, *343*, 183. (c) Ai X., Caffrey M. *Biophys. J.* **2000**, *79*, 394.
(5) (a) Lawrence, M. J. *Chem. Soc. Rev.* **1994**, *23*, 417. (b) Razumas, V.; Kanapienene, J.; Nylander, T.; Engstrom, S.; Larsson, K. *Anal. Chim. Acta* **1994**, *289*, 155.
(6) (a) Gruner, S. M. *J. Phys. Chem.* **1989**, *93*, 7562. (b) Larsson, K. *J. Phys. Chem.* **1989**, *93*, 7304.
(7) Schwarz, U. S.; Gompper, G. *Phys. Rev. Lett.* **2000**, *85*, 1472.
(8) Angelov, B.; Ollivon, M.; Angelova, A. *Langmuir* **1999**, *15*, 8225.
(9) Gustafsson, J.; Nylander, T.; Almgren, M.; Ljusberg-Wahren, H. *J. Colloid Interface Sci.* **1999**, *211*, 326.
(10) (a) Garstecki, P.; Holyst, R. *Langmuir* **2002**, *18*, 2519. (b) Garstecki, P.; Holyst, R. *Langmuir* **2002**, *18*, 2529.
(11) Marrink, S. J.; Tieleman, D. P. *J. Am. Chem. Soc.* **2001**, *123*, 12383.
(12) Clerc, M.; Dubois-Violette, E. *J. Phys. II* **1994**, *4*, 275.
(13) (a) Harper, P. E.; Gruner, S. M. *Eur. Phys. J. E* **2000**, *2*, 217. (b) Harper, P. E.; Gruner, S. M.; Lewis, R. N. A. H.; McElhaney, R. N. *Eur. Phys. J. E* **2000**, *2*, 229.
(14) Boulin, C. J.; Kempf R.; Gabriel, A.; Koch, M. H. *J. Nucl. Instrum. Methods* **1988**, *A269*, 312.
(15) da Graca Miguel, M.; Eidelman, O.; Ollivon, M.; Walter, A. *Biochemistry* **1989**, *28*, 8921.

JA034578V

Supplementary Material

Comparison of the cubic lattice parameters of monoolein/water and monoolein/octylglucoside/buffer-solution structures

Figure 1S shows the comparison of the thermal behavior of the Pn3m unit cell lattice parameter, *a*, of pure monoolein (MO) fully hydrated in water (filled triangles) with those of the presently investigated MO/OG (90/10, mol/mol) mixture hydrated in excess aqueous phase 0.1 M NaCl (phosphate buffer pH 7.0) (filled circles). The data for pure MO have been published in Czeslik C., Winter R., Rapp G., Bartels K., *Biophys.J.* **1995**, 68, 1423-1429. In excess water, the diamond type cubic lattice of pure MO transforms into a hexagonal phase at temperatures above 94 ^{o}C. Our dynamic X-ray scans established that the MO/OG cubic phase structure remains in the Pn3m space group symmetry up to 100 ^{o}C. The lattice spacing of the MO/OG cubic phase in buffer at 25 ^{o}C ($a_{(D_{Large})}$ = 15.1 nm) is by about 40% larger than that of pure MO in water ($a_{(D_{Normal})}$ = 10.7 nm) at same temperature.

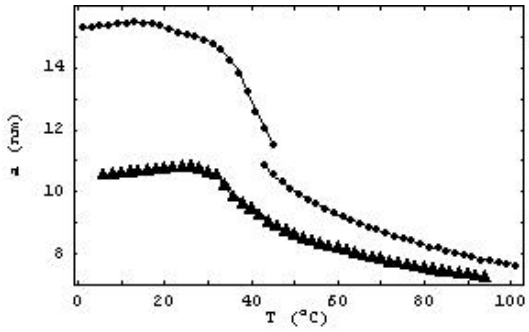

Figure 1S

Experimental synchrotron X-ray diffraction patterns of cubic MO/OG dispersions at selected temperatures and analysis of the X-ray reflections based on the GH model

Figure 2S shows experimental X-ray diffraction patterns of the investigated MO/OG mixture (90/10, mol/mol) at full hydration in 0.1 M NaCl phosphate buffer solution with pH 7. The presented frames were acquired at the indicated temperatures from a heating scan performed at a rate 2 ^{o}C/min from 1 to 100 ^{o}C. The scan rate was chosen after series of scans of MO/OG/water mixtures of various molar ratios. The investigated systems, including the one reported here, showed fast response to the temperature changes on heating.

The X-ray patterns recorded at temperatures 1 ^{o}C and 3 ^{o}C revealed that intensive reflections of a diamond type cubic lattice (space group Pn3m) overlap with low-intensity peaks of a primitive cubic lattice (space group Im3m). The green bars in Figure 2S index from left to right the positions of the maxima of the (110), (200), (211), (220), (310), (222), (321) and (400) reflections of an Im3m cubic lattice. The s-values of the peak maxima for Im3m cubic space group are spaced in the characteristic ratio $\sqrt{2} : \sqrt{4} : \sqrt{6} : \sqrt{8} : \sqrt{10} : \sqrt{12} : \sqrt{14} : \sqrt{16}$. The red bars in Figure 2S consecutively denote the (110), (111), (200), (211), (220), (221), and (310) reflections of a diamond cubic lattice. The X-ray peak set for a Pn3m cubic space group is identified by the characteristic ratio of the s-values of the diffraction maxima $\sqrt{2} : \sqrt{3} : \sqrt{4} : \sqrt{6} : \sqrt{8} : \sqrt{9} : \sqrt{10}$. The reflections of the primitive Im3m cubic phase vanished at temperatures above 5 ^{o}C.

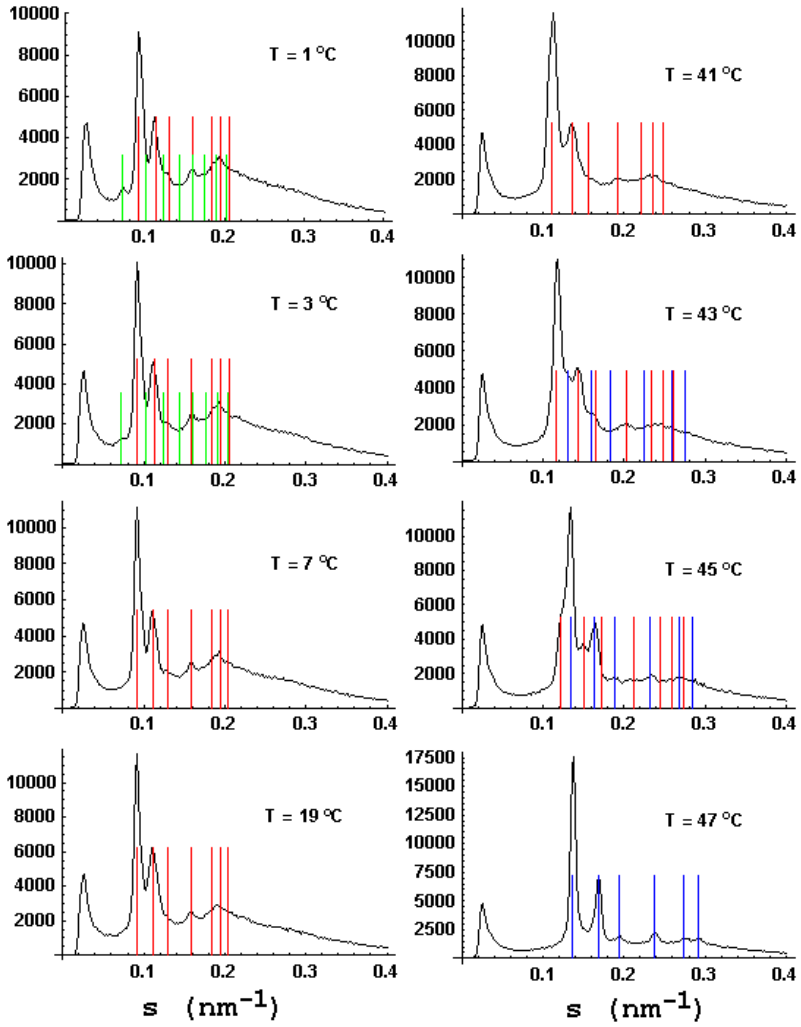

Figure 2S

The X-ray reflections recorded in the interval 5 ^{o}C < T < 100 ^{o}C were best fitted by a peak set typical for the diamond type cubic lattice (space group Pn3m). No other space group (from the presently known for cubic phases of hydrated amphiphiles) could better describe the experimentally observed X-ray diffraction peaks (Fig. 2S). Notably, a cubic-cubic structural transition was resolved to occur at temperature around 44 ^{o}C during the dynamic thermal scan. The positions of the Bragg peaks identifying the two diamond cubic lattices are indicated in Figure 2S by red (D_{Large}) and blue (D_{Normal}) bars, respectively.

A careful examination of the shape of the X-ray patterns at temperatures below 43 ^{o}C revealed remarkable differences with respect to the shape of the patterns at T > 45 ^{o}C. We established that at low temperatures the reflections of the diamond cubic lattice D_{Large}, characterized by a unit cell spacing around 15 nm, are superimposed on a large diffuse scattering with a maximum centered in the interval of spacings s~0.20÷0.25 nm^{-1} (see the green curves in Figures 3S and 4S at T= 19, 43 and 45 ^{o}C). At T < 43 ^{o}C, the diamond cubic phase, referred to as D_{Large} nonlamellar phase, displays Bragg peaks with larger widths and lower intensities as compared to the Bragg peaks resolved for the D_{Normal} cubic phase (Pn3m space group) at T > 45 ^{o}C.

During the heating scan, coexisting reflections of two diamond type cubic lattices were resolved at T = 43 ºC and T = 45 ºC (Figs. 2S and 4S). At T = 43 ºC, the peaks of the D_{Large} cubic phase (represented by red bars in Fig. 2S) are with stronger intensities as compared to those of the second cubic phase D_{Normal} (lower intensity peaks indexed in blue). At T = 45 ºC, the intensities of the peaks of the second diamond cubic phase (D_{Normal}) begin to increase, and at T > 47 ºC this nonlamellar phase is entirely dominating (see the peaks indexed by blue bars at T = 45 ºC and 47 ºC in Fig. 2S). Upon the growth of the D_{Normal} cubic phase, the intensity of the scattering background centered at s ~ 0.23 nm^{-1} diminishes by about 50% (see the green curve in Fig. 3S). At T > 45 ºC, the Bragg peaks of the D_{Normal} phase exhibited increased intensities and they were narrow in width. This indicates a longer-range correlation of the three-dimensional order at temperatures above the transition temperature 45 ºC.

Towards peaks fitting, the obtained diffraction patterns were normalized and the background was subtracted. Figures 3S and 4S show examples of the peak fitting. The red curves represent the Gaussian peak fitting for the D_{Large} cubic phase, the blue curves show the Gaussian peaks for the D_{Normal} cubic phase, and the green curves correspond to the diffuse scattering with maxima centered at s-spacings between 0.20 and 0.25 nm^{-1}.

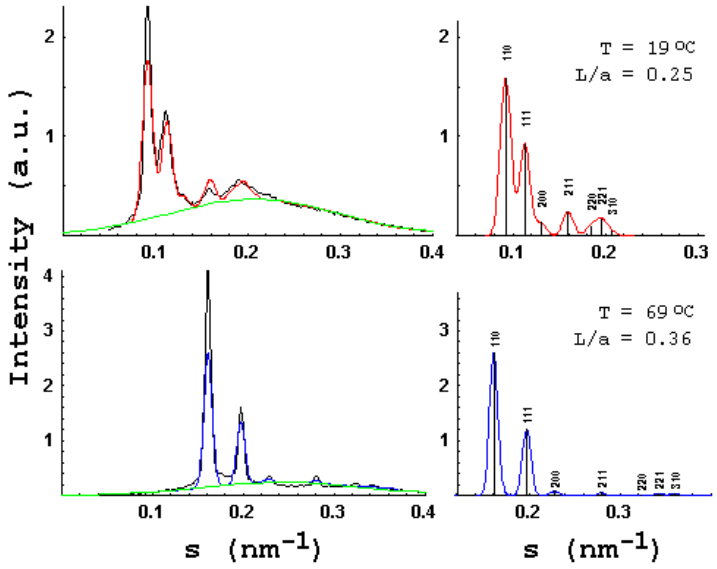

Figure 3S

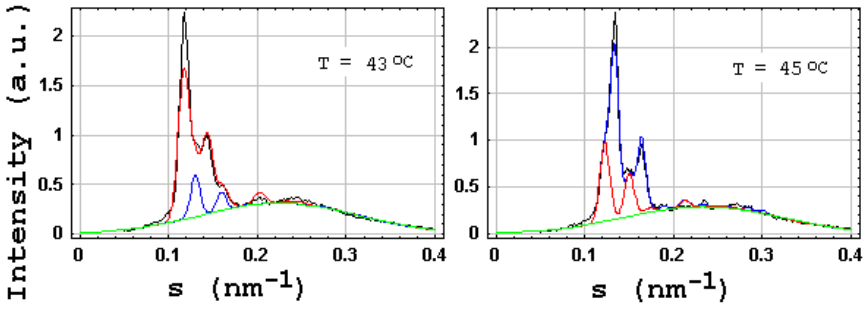

Figure 4S

Figure 3S presents the fitting of the X-ray patterns of the single diamond D_{Large} cubic phase at T = 19 °C (top red curves) and of the single diamond D_{Normal} cubic phase at T = 69 °C (bottom curves in blue). Figure 4S shows the peak fitting describing the cubic-cubic structural transition from D_{Large} to D_{Normal} phase. At 43 °C, the D_{Large} phase displays high-intensity reflections (red Gaussian peaks), while the D_{Normal} phase has been just nucleated upon the heating and displays low-intensity peaks (blue Gaussian curves). At 45 °C, the D_{Normal} peaks grow (blue Gaussian peaks), while the D_{Large} peaks vanish (red Gaussian peaks).

According to the theory of Gartecki and Hołyst[10] the relative intensities of the diffraction peaks for a given chemical composition depend on the thickness of the lipid bilayer, determining the distribution of the electron density in the 3D system. We determined the structural parameters of the diamond-type cubic lattices formed in fully hydrated MO/OG (90/10, mol/mol) mixture by a nonlinear regression. The lipid bilayer thickness, *L*, in the cubic lipid phase was estimated from the lattice parameter, a, on the basis of the GH model[10]. The intensities in the experimental X-ray patterns were fitted to model scattering intensities defined as

$$I_{hkl}^{(\mathrm{mod})}(\mathrm{L}) = M_{hkl}\left[F_{hkl}^{S*}\frac{\sin(\alpha_{hkl}\pi(h^2+k^2+l^2)^{1/2}L^*)}{\alpha_{hkl}\,{}_2\pi(h^2+k^2+l^2)^{1/2}}\right]^2 \qquad (1),$$

where $L^* = L/a$ is the dimensionless lipid layer thickness, F^{S*} is the dimensionless structure factor, M_{hkl} is a multiplicity factor, and α_{hkl} are correction parameters for particular cubic lattice types[10]. The shape of every reflection was modeled as a Gaussian peak with intensity calculated according to Eq. 1. For the practical realization, we used a multivariable nonlinear fitting procedure written as a Wolfram Mathematica notebook. The NonlinearRegress function from the package `NonlinearFit` was used (*Mathematica 3.0 Standard Add-on Packages*; Wolfram Research, Inc.; Cambridge University Press: Cambridge, 1996). It allowed us to perform an improved fitting.

Figure 3S clearly shows that the intensities of the (110), (111), (200), (211), (220), (221), and (310) reflections of the D_{Large} (L/a = 0.25) cubic lattice are not spaced in the same peak intensity ratio as those for the D_{Normal} (L/a = 0.36) cubic phase. The higher-order peaks of the D_{Normal} cubic phase appear to be with negligibly small intensities as compared to its first order reflection (110) (Fig. 3S). While preserving same indexing of the Bragg peaks in the D_{Large} and D_{Normal} patterns, the temperature-induce change in the sample chemical composition (reflecting the OG solubility in the MO matrix), as well as the associated changes in the lipid bilayer thickness and lipid hydration, causes an alteration of the electron density distribution in the nonlamellar 3D structure, which results in different relative peak intensities of the D_{Large} and D_{Normal} phases.

The results obtained for the lipid bilayer thickness, *L*, water channel thickness, D_W, and the cubic lattice parameters $a_{(D_{Large})}$ and $a_{(D_{Normal})}$ are given in Table 1S for selected temperatures (see the X-ray patterns in Figures 3S and 4S). D_W was calculated by the equation: $D_W = 0.707\,a - L$. The obtained bilayer thickness for the "normal" cubic phase is in accord with that for the pure MO. The established temperature dependence of the dimensionless bilayer thickness is smaller for the "normal" cubic lattice as compared to that for the "large" one. This feature probably results from the temperature variation of the cubic lattice constant, *a,* and the geometrical packing constraints of the two lipid monolayers in the bilayer. The diamond type cubic phase is the most stable bicontinuous amphiphilic cubic phase existing in excess water. This study demonstrated that it is capable of preserving a 3D nanoperiodicity of the cubic Pn3m space group in its swollen state in the presence of OG.

Table 1S

Temperature	**19 ^{o}C**	**43 ^{o}C**	**45 ^{o}C**	**69 ^{o}C**
$a_{(D_{Large})}$ [nm]	15.35	12.06	11.54	--
$a_{(D_{Normal})}$ [nm]	--	10.87	10.56	8.77
$L_{(D_{Large})}$ [nm]	3.84	3.6	3.44	--
$L_{(D_{Normal})}$ [nm]	--	3.99	3.92	3.2
D_W [nm] (D_{Large})	7.01	4.92	4.72	--
D_W [nm] (D_{Normal})	--	3.69	3.55	3.0